



Preparation of core-shell TiO₂@ZIF-67 and its effective adsorption of methyl orange from water

Jingli Zhang^{a,b,*}, Xi Yang^{a,b}, Shuijie Cheng^{a,b}, Decheng Zou^{a,b}, Fang Cheng^{a,b}

^aSchool of Environmental and Municipal Engineering, Tianjin Chengjian University, Tianjin 300384, China, Tel. +86 22 23085117; emails: jinglizhangczp@126.com (J. Zhang), 1546043363@qq.com (X. Yang), 3289504809@qq.com (S. Cheng), 494008425@qq.com (D. Zou), chengfang10@sina.com (F. Cheng)

^bTianjin Key Laboratory of Aquatic Science and Technology, Tianjin Chengjian University, Tianjin 300384, China

Received 7 September 2021; Accepted 6 April 2022

ABSTRACT

The TiO₂@ZIF-67 nanocomposite, flower-like ZIF-67 coated on the surface of anatase TiO₂, was prepared by solvothermal method for the first time. The TiO₂@ZIF-67 was characterized by various techniques such as scanning electron microscopy, Fourier-transform infrared spectroscopy, and X-ray diffraction. The removal efficiency of methyl orange (MO) onto TiO₂@ZIF-67, TiO₂ and ZIF-67 was 94.01%, 14.77% and 47.08% with the corresponding adsorption capacity of 5.87, 0.875 and 2.94 mg g⁻¹ in 50 mL solution with low MO content of 5 mg L⁻¹, respectively. The adsorption capacity of TiO₂@ZIF-67 changed a little in the pH range of 4–8 and its adsorption kinetics conformed to the quasi-second-order equation. The MO adsorption onto TiO₂@ZIF-67 was an exothermic reaction and the equilibrium adsorption capacity rose with the increase of temperature. The effective adsorption resulted from electrostatic force, π - π stacking, acid-base interaction, and the hydrogen bond formed by water as bridge. The adsorbent was regenerated easily by putting into alkaline aqueous solution (pH = 12) and the adsorption of TiO₂@ZIF-67 decreased a little for five cycles.

Keywords: TiO₂@ZIF-67; Methyl orange; Adsorption; Reuse

1. Introduction

Azo dyes, a class of synthetic dyes containing the azo group (-N=N-) in molecular structure, are widely used in textile industry, color photography, leather fine manufacturing, pharmaceutical industry, cosmetics production and other fields [1,2]. The azo dyes are harmful to environment and organism. Azo dyes in water can absorb light and decrease photosynthesis of aquatic plants [3] which can yield dissolved oxygen in water body. Azo dyes could also be absorbed and accumulated by aquatic plants [2] and cause distortion and even death of aquatic organisms [3]. Furthermore, azo dyes are not easy to be degraded completely [4]. Acute exposure to methyl orange (MO) can

increase heart rate and cause many diseases such as tissue necrosis, jaundice and cyanosis for humans [5].

The treatment of dyeing wastewater includes adsorption, membrane [6–8], coagulation–flocculation [8], photocatalysis [9,10], electrochemical [11] and biological methods [12]. Membrane, photocatalysis and electrochemical method have many disadvantages such as high investment cost and operation cost. Precipitation and coagulation often consume massive chemicals and engender a large amount of sludge need to be treated. Azo dyes degrade slowly and often produce more toxic intermediates for biological methods [12]. Adsorption is a preferred technique to these other methods for MO removal due to its simple design, easy operation, high removal efficiency, low operation cost and no other contaminant production [13].

* Corresponding author.

TiO₂ is an excellent semiconductor photocatalytic material due to its non-toxic, good biocompatibility, good thermal and chemical stability, and high mechanical strength with low adsorption performance [10]. The adsorption capacity of TiO₂/GO composite prepared by the ultrasonic activation is greatly improved as compared with pure TiO₂ [14]. Metal-organic framework (MOFs), an emerging material, show extraordinary super advantages in the field of adsorption due to their high specific surface area, porous structure, unsaturated metal active sites, large number of Lewis acid sites. The adsorption capacity of the composite, a ZIF-8 decorated TiO₂ grid-like film by in-situ growth method, is much higher than that of pure TiO₂ film, and the increase of substrate concentration on the surface of photocatalyst is also conducive to the process of catalytic reaction [15].

MO, well-known as an indicator for pH titration, is a widely used dye in the textile industry and was chosen as target pollutant in this study. ZIF-67, an important MOF, has good water and chemical stability and good adsorption [16]. Co²⁺, the central ion in ZIF-67, can also link with -SO₃ in MO [17]. In order to improve the adsorption performance, the compound material TiO₂@ZIF-67, TiO₂ coated with ZIF-67, was synthesized by solvent-thermal synthesis after the anatase TiO₂ was prepared by sol-gel method in this work. And then the adsorption behavior and adsorption mechanism of MO onto TiO₂@ZIF-67 were investigated.

2. Chemical reagents and material preparation

2.1. Chemical reagents

Ultrapure deionized water adopted in our experiment was total organic carbon of 1.2 μg L⁻¹, resistivity of 1.82 MΩ cm at 25°C. Titanium(IV) butoxide (TBOT) was gotten from Fuchen Chemical Reagent Limited Company (Tianjin, China) and other reagents were purchased from Jiangtian Chemical Company (Tianjin, China). Analytically pure reagents without further treatment was used in this study.

2.2. Synthesis of three materials

TiO₂ was prepared in accordance with the modified Tan's method [18]. In brief, TBOT was added into 0°C deionized water (the molar ratio of water to TBOT is 100:1) and stirred. The white precipitate was washed 3 times with deionized water after it was collected by filtering. The precipitate were added into deionized water at the temperature of 50°C for 3 h ageing, and then dried out at 110°C in air oven for overnight. Finally, the TiO₂ product was gotten by calcining in muffle furnace at 450°C for 2 h after being carefully grinded.

The method of as-synthesized ZIF-67 followed our work [19] with some changes. In detail, 1.1642 g C₆O(NO₃)₂·6H₂O and 1.3136 g 2-methylimidazole dissolved in 15 mL methanol separately with 0.5 h ultra-sonication for, labeled as liquid A and liquid B. And then liquid A and B were ultra-sonicated for 2 h after mixing together. ZIF-67 was obtained after purple material collected was washed three times in methanol and dried in 60°C vacuum.

The first step of TiO₂@ZIF-67 synthesis was the same as ZIF-67 preparation except that 0.3 g TiO₂ was dispersed in

solution A before the purple material was obtained. And then the purple material was mixed with new solution A once again. The mixed liquid was poured to a seal stainless reactor with Teflon lining, and then kept under 120°C for 2 h [20]. When the reactor cooled down to room temperature, the precipitates were processed as ZIF-67 washing and drying. The light yellow-green TiO₂@ZIF-67 powder was obtained.

2.3. Analytical methods

The MO concentration was determined at wavelength of 464 nm by H. UV-Vis spectrophotometer (T6, Beijing Puxi General Instrument Co., Ltd., China). The appearances of the synthesized materials were monitored by a scanning electron microscopy (SEM, Gemini SEM500, Germany). The X-ray diffraction (XRD) patterns were determined using a diffractometer (Ultima IV, Rigaku, U.S.) with mono-chromatized Cu Kα under 40 kV and 40 mA. And the 2θ for diffraction data were changed from 5° to 80° with the step of 0.02°. The functional groups were detected by Fourier-transform infrared spectroscopy (FTIR, Equinox 55, Germany) in a spectrum range of 400–4,000 nm. The surface potential and particle size were measured by Malvern Zetasizer Nano ZS 90 (UK). The specific surface area and pore volume was measured using Brunauer–Emmett–Teller method (BET) by NovaWin Version 10.01 (Quantachrome, USA).

2.4. MO adsorption

The adsorption of MO onto adsorbents was performed in sequencing batch mode. The material was put into 50 mL MO solution with a set concentration, and then the mixed liquor was shaken using a constant temperature shaker. The adsorption capacity of material is obtained from Eq. (1).

$$Q_t = \frac{(C_0 - C_t)v}{m} \quad (1)$$

where C_{t_0} is adsorbate concentration at time t or 0, v (L) is the volume of adsorbate solution and m is adsorbent mass. Q_t and Q_e (mg g⁻¹) are the adsorption capacity at t time and at equilibrium, respectively. The removal rate is calculated as follows:

$$\eta = \frac{(C_0 - C_e)}{C_0} \times 100\% \quad (2)$$

where η is the removal rate.

3. Results and discussion

3.1. Characterization

The three as-synthesized materials of TiO₂, ZIF-67 and TiO₂@ZIF-67 were monitored by SEM, XRD and FTIR. TiO₂ is a spherical particle with size of 200–500 nm (Fig. 1). ZIF-67 had a perfect dodecahedral rhombic morphology with the particle size of about 200–400 nm (Fig. S1), which is a

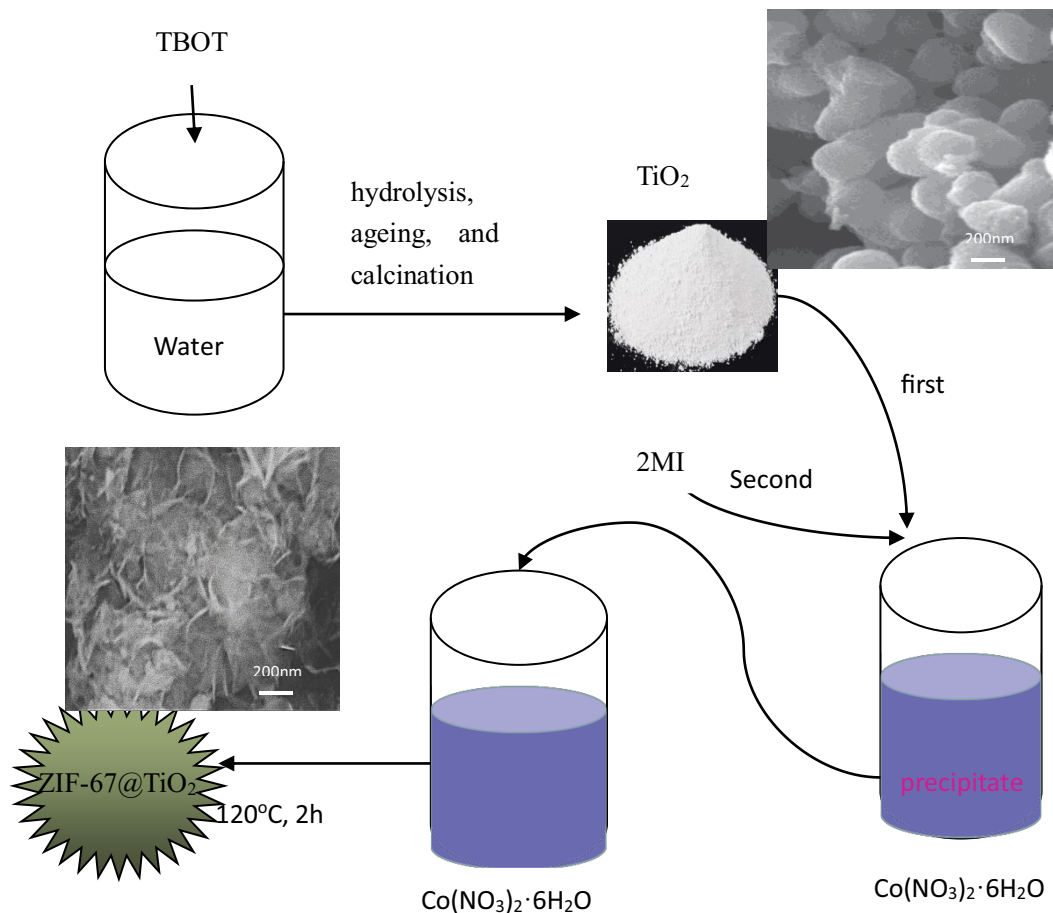


Fig. 1. Schematic of $\text{TiO}_2@\text{ZIF-67}$ synthesis process.

little than that in our previous work [19]. That is probably due to shorter reaction time. $\text{TiO}_2@\text{ZIF-67}$ showed that the flower-like ZIF-67 was grown on the surface of spherical TiO_2 (Fig. 1).

The XRD patterns of the three materials are shown in Fig. 2a. The 2θ of 7.31° , 10.42° , 12.78° , 14.76° , 16.50° , 18.08° , 22.18° , 24.54° , 25.64° , 26.7° , 29.74° , 30.64° , 31.50° , and 32.42° in the XRD pattern of ZIF-67 represented the crystal face of (011), (002), (112), (022), (013), (222), (114), (233), (224), (134), (044), (334), (244) and (235) [19], and the 2θ of 25.56° , 38.14° , 48.12° , 54.06° , and 55.24° in TiO_2 XRD pattern represented the crystal face of (101), (112), (200), (105) and (211) [20]. The diffraction peaks of $\text{TiO}_2@\text{ZIF-67}$ are in good agreement with these of ZIF-67 and TiO_2 , showing that it was successfully synthesized (Fig. 2a).

The wide vibration band about 488 cm^{-1} from the FTIR spectra of TiO_2 (Fig. 2b) is the typical vibration peak of Ti–O–Ti bond of TiO_2 , indicating that TiO_2 is successfully synthesized [21,22]. The vibration peaks from 600 to $1,500\text{ cm}^{-1}$ in the FTIR spectra of ZIF-67 can be attributed to the stretching vibration of imidazole ring, and the peaks at $1,385$, $1,631$ and $3,130\text{ cm}^{-1}$ are caused by the stretching vibration of C–N bond, C=N bond and C–H bond of ligand imidazole in ZIF-67, respectively [20,23]. The vibration peak of $\text{TiO}_2@\text{ZIF-67}$ was similar to ZIF-67. That conformed to the

result of XRD pattern and further proved that ZIF-67 was successfully loaded on the surface of the TiO_2 .

3.2. MO adsorption experiments

3.2.1. MO adsorption onto three materials

TiO_2 , ZIF-67 and $\text{TiO}_2@\text{ZIF-67}$ (0.04 g) were added into 5 mg L^{-1} MO solution at temperature of 25°C , respectively. As shown in Fig. 3a, the removal efficiency of MO onto $\text{TiO}_2@\text{ZIF-67}$ was 94.01%, which was approximately 6.4 times of TiO_2 (14.77%) and 2.0 times of ZIF-67 (47.08%). The adsorption equilibrium time was $\text{TiO}_2@\text{ZIF-67} > \text{ZIF-67} > \text{TiO}_2$. Comparing with other adsorbents (Table S1), ZIF-67 has the maximum capacity Q_{max} ($1,340\text{ mg g}^{-1}$) of MO sorption calculated from Langmuir isotherm [19]. The removal efficiency of MO by $\text{TiO}_2@\text{ZIF-67}$ was much higher than ZIF-67, showing it had super high adsorption capacity for MO.

3.2.2. Effect of dosage

$\text{TiO}_2@\text{ZIF-67}$ with dosage of 0.02, 0.04, 0.06, 0.08 and 0.10 g was added into 5 mg L^{-1} MO solution for 15 h at 25°C , respectively. The results are shown in Fig. 3b. When the dosage increased the equilibrium concentration and adsorption capacity both decreased. Although the adsorption sites rose

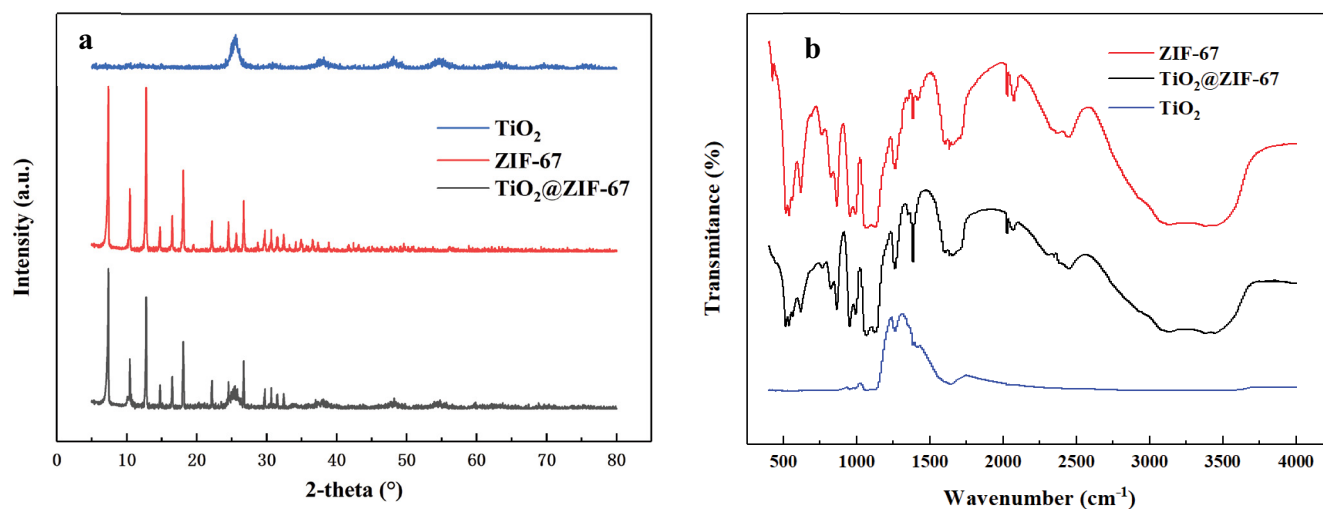


Fig. 2. (a) XRD patterns and (b) FTIR spectra of the prepared ZIF-67, TiO₂ and TiO₂@ZIF-67.

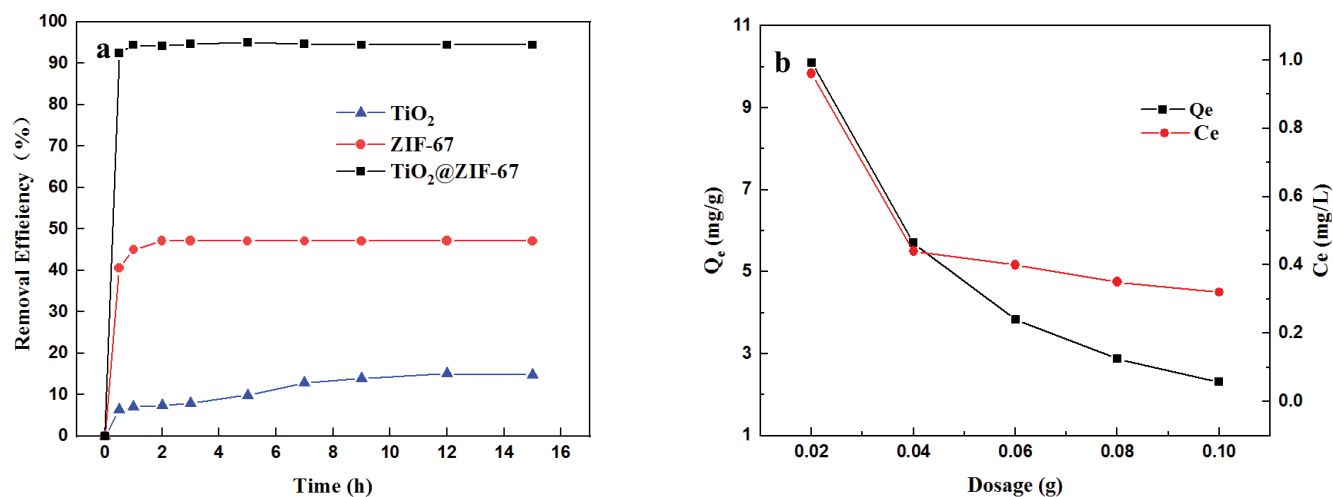


Fig. 3. (a) Removal efficiency of MO at different times by the three materials and (b) MO adsorption of TiO₂@ZIF-67 dosages.

with the increase of adsorbent dosage, the average amount of pollutants captured by the adsorption sites decreased. The adsorption equilibrium concentration decreased a little when the adsorbent dosage was changed from 0.04 to 0.10 g. Therefore, the dosage of TiO₂@ZIF-67 was adopted 0.04 g in the later experiments.

3.2.3. Effect of initial pH

pH always has an essential effect on adsorption. The range of pH is from 4 to 12 in our experiment at 25°C. The pH of MO solution was changed a set value by adding 0.1 mol L⁻¹ HCl or NaOH. The equilibrium adsorption capacity Q_e decreased a little when pH was increased from 4 to 8 and the largest Q_e was 5.93 mg g⁻¹ at pH = 4 (Fig. 4). When the pH value changed from 10 to 12, the Q_e decreased sharply. The result showed that it is much more favorable for MO removal under acidic condition. The reason was analysed in Section 3.5 – Adsorption thermodynamics. The pH value of MO solution was not adjusted in the follow-up experiments because it is approximately 6.5.

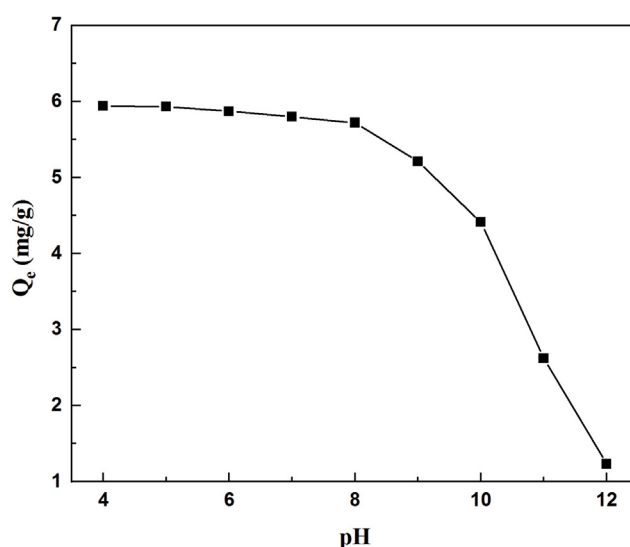


Fig. 4. MO adsorption on TiO₂@ZIF-67 at different initial pHs.

3.3. Adsorption kinetics analysis

TiO₂@ZIF-67 was put into MO solution with different MO concentration of 1, 2.5 and 5 mg L⁻¹ at 25°C for adsorption kinetics study. Samples were filtrated by 0.22 μm membrane before MO concentration was detected at t time. The adsorption capacity is close to the equilibrium value with each concentration about 1 h. The MO adsorption onto TiO₂@ZIF-67 is a fast process (Fig. 5a).

Since the first-order kinetic model could not fit the experimental data well (Supporting Information Part S1), the second-order model was adopted to study the sorption mechanism and the expression of the second-order kinetic model could be expressed as [25].

$$\frac{t}{Q_t} = \frac{1}{k_2 \cdot Q_e^2} + \frac{t}{Q_e} \quad (3)$$

where k_2 (g mg⁻¹ h⁻¹) is adsorption rate constant. The second-order kinetic model could fit the adsorption experimental data well because all their R^2 values were above 0.999 and the calculated values of equilibrium capacity were close to the experimental data (Fig. 5b and Table S3). Therefore, it could be preliminarily judged that there is a chemical adsorption of electron pair sharing or electron transfer in the whole adsorption process.

3.4. Adsorption isotherm analysis

The isotherm models can be adopted not only to describe the relationship between the adsorbate concentration and the equilibrium adsorption capacity at a set temperature, but also to design the adsorption system [26]. The experiments were performed putting TiO₂@ZIF-67 into MO solution with various initial MO concentrations of 1, 2.5, 5, 7.5 and 10 mg L⁻¹ at temperatures of 25°C, 35°C and 45°C, respectively. The results are seen from Fig. 6. When the

temperature rose the equilibrium MO concentration became larger and the adsorption capacity became smaller. The equilibrium adsorption concentration at 45°C (2.54 mg L⁻¹) was 5 times as much as that at 25°C (0.51 mg L⁻¹) at MO initial concentration of 10 mg L⁻¹. That indicated that lower temperatures was favorable the MO adsorption onto TiO₂@ZIF-67.

In order to further explore the relationship between temperature and adsorption, Langmuir, Freundlich and Henry models were fitted to experimental data, as the parameters of these models are practical, simple and easy to explain [27]. Langmuir model could not fit the data well (Supporting Information Part S2). Freundlich model is widely employed to express the surface sorption with sites having different adsorption energies. Freundlich model is as follow [28]:

$$\ln Q_e = \frac{1}{n} \ln C_e + \ln K_F \quad (4)$$

where K_F is Freundlich isotherm constant, and $1/n$ is the Freundlich intensity parameter which shows the adsorption intensity or the heterogeneity of adsorbent surface. Freundlich model could fit the adsorption data well (Fig. 6b and Table 1), for R^2 values were 0.995, 0.996, and 0.995 at temperatures of 25°C, 35°C and 45°C, respectively. The value of $1/n$ ranges from 0 to 10 for favorable adsorption [29]. TiO₂@ZIF-67 had strong adsorption intensity due to the $1/n$ value of 1.050 at 25°C, 1.200 at 35°C and 1.392 at 45°C (Table 1). The value of $1/n$ got smaller and the value of K_F turned larger at higher temperature, demonstrating that the adsorption got weaker and the capacity became smaller [27].

Henry model is:

$$Q_e = K_p C_e \quad (5)$$

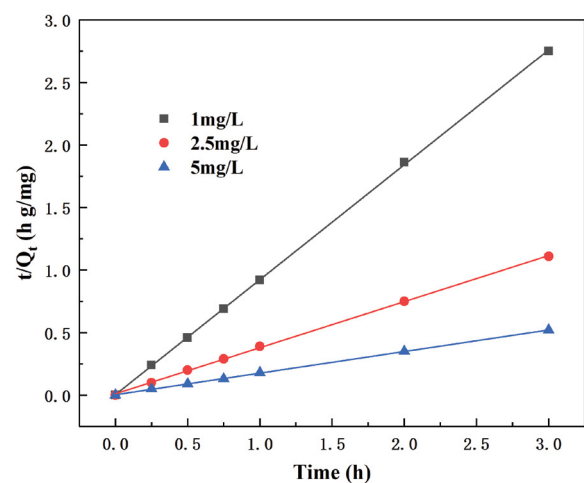
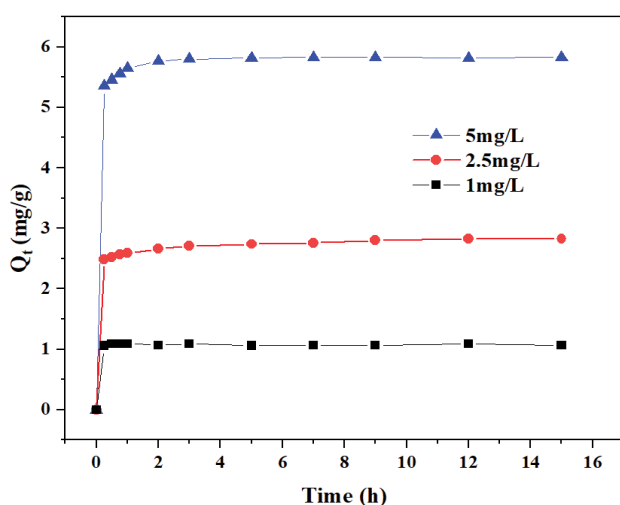


Fig. 5. Adsorption of MO onto TiO₂@ZIF-67 (a) at various times and initial concentrations and (b) fitting the second-order kinetic model.

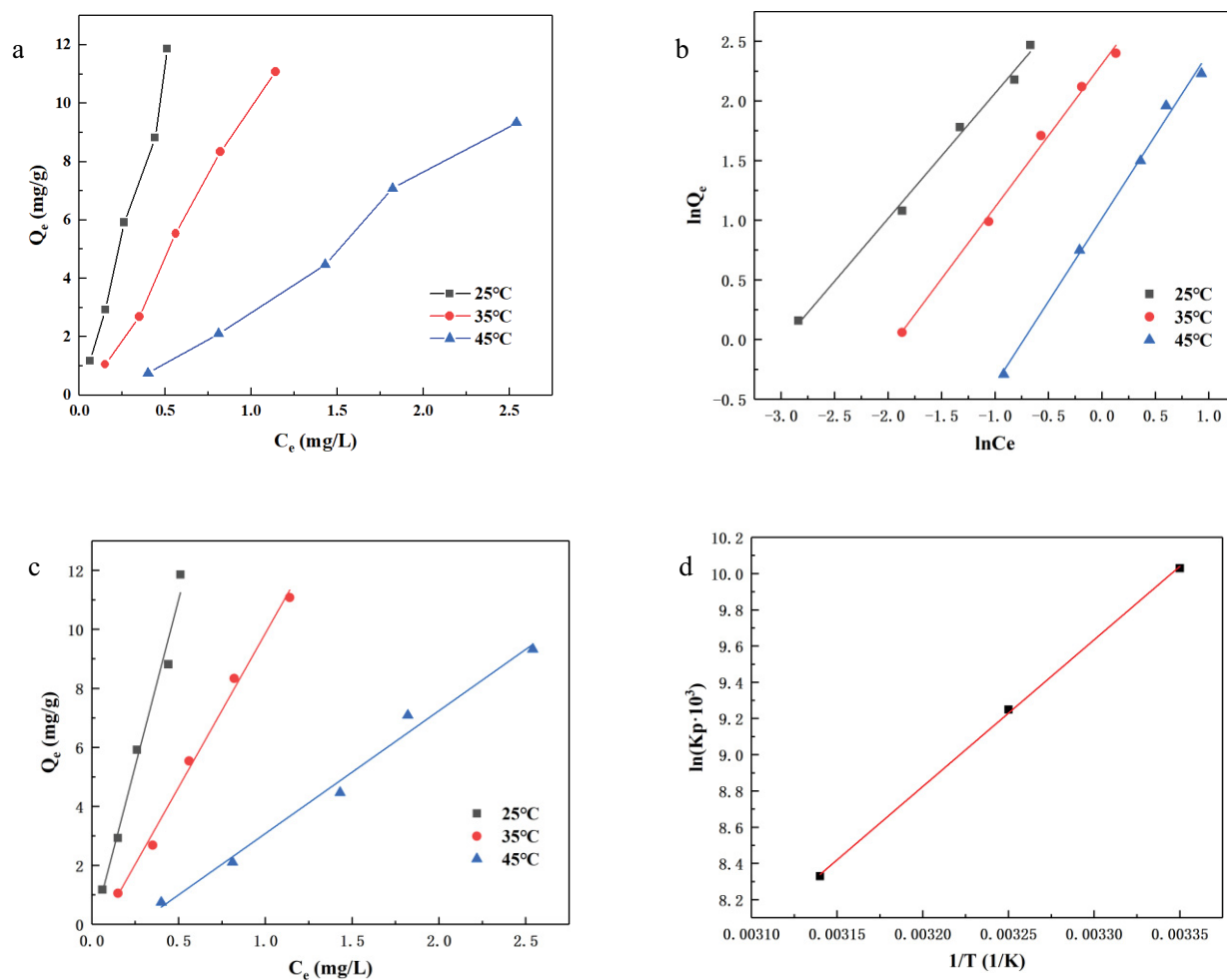


Fig. 6. (a) MO adsorptions onto TiO₂@ZIF-67 at various temperatures, fitting the models for (b) Freundlich and (c) Henry of MO sorption on TiO₂@ZIF-67, and (d) van't Hoff plot.

where K_p (L g⁻¹) is sorption constant. Henry model is suitable to fit to experimental data with all $R^2 \geq 0.95$ (Fig. 6c and Table 1).

3.5. Adsorption thermodynamics

In order to explore the effect of temperature on the MO sorption on TiO₂@ZIF-67, the experimental data were analyzed thermodynamically at temperatures of 25°C, 35°C and 45°C. The fitting parameters of thermodynamic models are shown in Table 1. The distribution constant K_p gotten from the Henry model was adopted in thermodynamic analysis. The coefficient K_p (L g⁻¹) obtained from the Henry model, could be converted to a dimensionless constant by multiplying K_p by a factor of 1,000 [29], so ΔG , ΔH and ΔS can be obtained by the following formulae.

$$\Delta G = -RT \ln(K_p \times 10^3) \quad (6)$$

$$\ln(K_p \times 10^3) = -\frac{\Delta H}{RT} + \frac{\Delta S}{R} \quad (7)$$

Table 1

Parameters of MO adsorption on TiO₂@ZIF-67 for thermodynamic analysis

Temperature	(°C)	25	35	45
Langmuir model	Q_{max} (mg g ⁻¹)	-71.327	-20.004	-8.624
	K_L (L mol ⁻¹)	-0.281	-0.342	-0.225
	R^2	0.236	0.715	0.780
Freundlich model	$1/n$	1.050	1.200	1.392
	K_F	22.529	10.078	2.769
Henry model	R^2	0.995	0.996	0.995
	K_p (L g ⁻¹)	22.601	10.440	4.160
ΔG	(kJ mol ⁻¹)	-24.850	-23.687	-22.032
ΔS	(kJ mol ⁻¹ K ⁻¹)	-0.142		
ΔH	(kJ mol ⁻¹)	-67.335		

where ΔG (kJ mol⁻¹) is the change of molar Gibbs function, ΔH (kJ mol⁻¹) is enthalpy change and ΔS (kJ mol⁻¹ K⁻¹) is entropy change. R , a universal gas constant, is 8.314 J mol⁻¹ K⁻¹ and T (K) is Kelvin temperature. The correlation coefficient

of $\ln(K_p \times 10^3)$ vs. $1/T$ was 0.999 (Fig. 6d) by fitting the van't Hoff isotherm model and then ΔH and ΔS were calculated from the slope and intercept of van't Hoff plot. The thermodynamic parameters of MO sorption onto $\text{TiO}_2@ZIF-67$ are shown in Table 1. All the ΔG values were negative at 25°C, 35°C and 45°C. The value becomes smaller with the temperature enhancement, demonstrating that the sorption of MO to $\text{TiO}_2@ZIF-67$ was a spontaneous process and the lower temperature was more conducive to the adsorption. ΔH ($-67.335 \text{ kJ mol}^{-1}$) < 0 , indicated that the MO adsorption onto $\text{TiO}_2@ZIF-67$ is an exothermic reaction. ΔS ($-0.142 \text{ kJ mol}^{-1} \text{ K}^{-1}$) was negative, showing that the randomness of MO molecule decreases with the MO sorption on $\text{TiO}_2@ZIF-67$ surface from its dissolved state.

3.6. Adsorption mechanism

The adsorption of MO onto ZIF-67 resulted from electrostatic force, acid-base action, π - π stacking, hydrogen bonding and ligand binding [30–32]. According to the zeta potential diagram (Fig. 7), the isoelectric points of ZIF-67

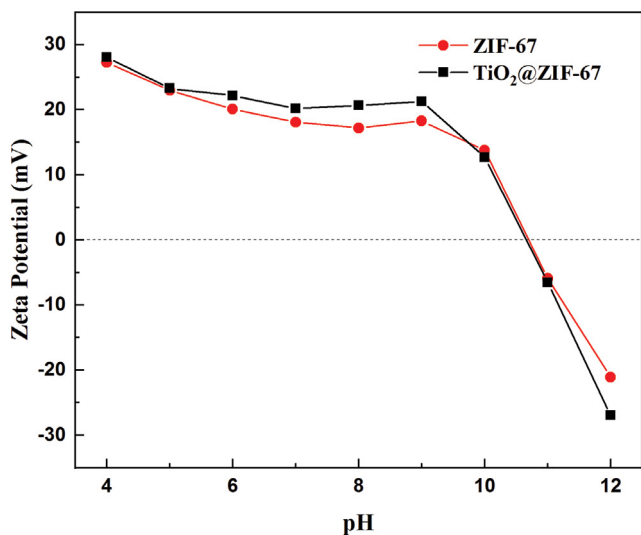


Fig. 7. Zeta potentials of ZIF-67 and $\text{TiO}_2@ZIF-67$ at various pHs.

and $\text{TiO}_2@ZIF-67$ are both at pH of 10.7. The surface potentials of the two adsorbents were positive at pH < 10.7 while they both were negative at pH > 10.7 . MO is an anionic dye ($\text{pK}_a = 3.4$) with the sulfonic acid group ($-\text{SO}_3^-$). When the pH was less than 10.7, there is the electrostatic attraction between the adsorbent and MO. The equilibrium adsorption capacity sharply decreased when the pH value changed from 9 to 12 (Fig. 4) because the deprotonation of functional groups on $\text{TiO}_2@ZIF-67$ made the $\text{TiO}_2@ZIF-67$ surface turn electronegative and improved the electrostatic repulsion. The imidazole ring of ZIF-67 has π - π stacking interaction with the benzene ring of MO molecule. The Lewis acidity of Co^{2+} in ZIF-67 could interacted with the Lewis basicity of $-\text{SO}_3^-$ group in MO [33,34]. Those showed the chemisorption played a predominant role in MO sorption onto $\text{TiO}_2@ZIF-67$. Furthermore, the double hydrogen bond, formed by the water molecule acting as the bridge, is also one of the driving forces for the adsorption (Fig. 8).

TiO_2 and $\text{TiO}_2@ZIF-67$ were mesoporous while ZIF-67 was microporous and the specific surface area (SSA), pore volume and mean pore diameter of $\text{TiO}_2@ZIF-67$ increased a little comparing with TiO_2 but its SSA was far less than ZIF-67 (SM Part S3). In our work, that the mixture was heated at 120°C for 2 h in $\text{Co}(\text{NO}_3)_2 \cdot 6\text{H}_2\text{O}$ solution improved Co^{2+} content, making the surface positive charge more abundant, and turned the rhombohedra dodecahedral ZIF-67 crystal on TiO_2 surface to flower-like appearance, causing the imidazole ring of ZIF-67 to become easier to get in touch with the benzene ring in dye molecules. Moreover, that the more unoccupied Co^{2+} of ZIF-67 interacted with $-\text{SO}_3^-$ of the dyes increased. Therefore, the adsorption capacity of $\text{TiO}_2@ZIF-67$ was much greater than pure ZIF-67 and TiO_2 .

3.7. Recycling

The regeneration and reuse of the adsorbent is crucial for its engineering practice. When the pH increased to 12, the adsorption capacity decreased sharply (Section 3.2.3 – Effect of initial pH). The regeneration method of the adsorbent in this work was gotten according to the characteristics. The saturated adsorbent was put into the aqueous solution (pH = 12) and washed for 3 times at room temperature. The 20 mL alkaline solution was used in all. The regenerated

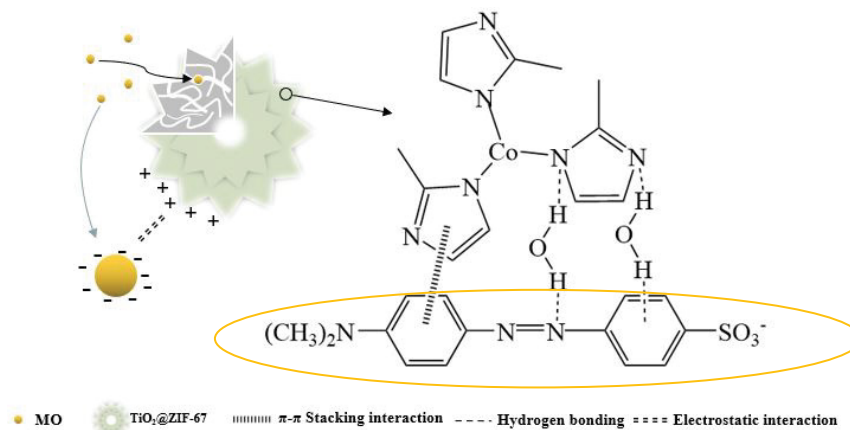


Fig. 8. Adsorption mechanism analysis for MO onto $\text{TiO}_2@ZIF-67$.

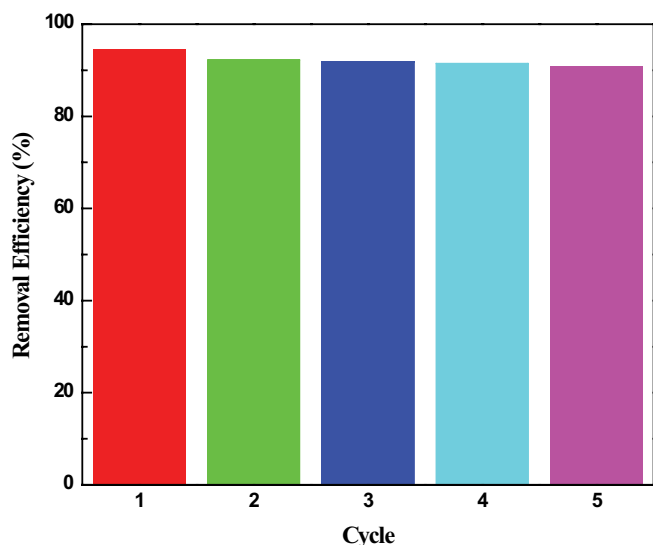


Fig. 9. TiO₂@ZIF-67 recycling for MO sorption.

adsorbent collected by centrifugation was washed by deionized water and methanol and then dried in vacuum dryer at 60°C. The adsorption of regenerated adsorbent is shown in Fig. 9. The removal rate of MO by TiO₂@ZIF-67 was maintained at about 90% in 5 cycles. The regeneration method can simply and effectively realize the separation and enrichment of MO.

4. Conclusion

In this work, the flower-like TiO₂@ZIF-67 (size: 400–500 nm) was successfully prepared by solvo-thermal method. Compared with TiO₂ and ZIF-67, TiO₂@ZIF-67 had highest removal rate (above 94%) in low-concentration MO solution. The adsorption of MO onto TiO₂@ZIF-67 was spontaneous and exothermic. The effective removal of MO by TiO₂@ZIF-67 adsorption was achieved by electrostatic force, π - π stacking, hydrogen bonds formed by water molecules as bridges, and more reaction sites due to the flower-like shape TiO₂@ZIF-67. The adsorbent as-synthesized in this study could be recycled by alkaline solution easily. The MO adsorption capacity still exhibited 90% after fifth cycle. The TiO₂@ZIF-67 is a good adsorbent with great potential for MO and also promising for the improvement of subsequent catalytic process.

CRedit authorship contribution statement

Jingli Zhang: Writing – review, editing and supervision, Xi Yang: Methodology, experiment, Decheng Zou: Writing – original draft and experiment, and Fang Cheng, Investigation.

Declaration of competing interest

The authors declare that they have no known competing financial interests or personal relationships that could have appeared to influence the work reported in this paper.

Acknowledgments

This work was supported by the National Natural Science Foundation of China (Grant number 51078265).

References

- [1] B.J. Brüsweiler, C. Merlot, Azo dyes in clothing textiles can be cleaved into a series of mutagenic aromatic amines which are not regulated yet, *Regul. Toxicol. Pharm.*, 88 (2017) 214–226.
- [2] Q. Zhou, Chemical pollution and transport of organic dyes in water-soil-crop systems of the Chinese coast, *Bull. Environ. Contam. Toxicol.*, 66 (2001) 784–793.
- [3] Y. Hou, S. Yan, G. Huang, Q. Yang, S. Huang, J. Cai, Fabrication of N-doped carbons from waste bamboo shoot shell with high removal efficiency of organic dyes from water, *Bioresour. Technol.*, 303 (2020) 122939, doi: 10.1016/j.biortech.2020.122939.
- [4] Y. Zhou, J. Lu, Y. Zhou, Y. Liu, Recent advances for dyes removal using novel adsorbents: a review, *Environ. Pollut.*, 252 (2019) 352–365.
- [5] A. Darwish, M. Rashad, H.A. AL-Aoh, Methyl orange adsorption comparison on nanoparticles: isotherm, kinetics, and thermodynamic studies, *Dyes Pigm.*, 160 (2019) 563–571.
- [6] A.B. Fradj, A. Boubakri, A. Hafiane, S.B. Hamouda, Removal of azoic dyes from aqueous solutions by chitosan enhanced ultrafiltration, *Results Chem.*, 2 (2020), doi: 10.1016/j.rechem.2019.100017.
- [7] F.R. Omi, M.R. Choudhury, N. Anwar, A.R. Bakr, M.S. Rahaman, Highly conductive ultrafiltration membrane via vacuum filtration assisted layer-by-layer deposition of functionalized carbon nanotubes, *Ind. Eng. Chem. Res.*, 56 (2017) 8474–8484.
- [8] N.C.L. Beluci, G.A.P. Mateus, C.S. Miyashiro, N.C. Homem, R.G. Gomes, M.R. Fagundes-Klen, A.M.S. Vieira, Hybrid treatment of coagulation/flocculation process followed by ultrafiltration in TiO₂-modified dye membranes to improve the removal of Reactive black 5 dye, *Sci. Total Environ.*, 664 (2019) 222–229.
- [9] M. Naushad, G. Sharma, Z.A. Allothman, Photodegradation of toxic dye using Gum Arabic-crosslinkedpoly (acrylamide)/Ni(OH)₂/FeOOH nanocomposites hydrogel, *J. Cleaner Prod.*, 241 (2019) 118263, doi: 10.1016/j.jclepro.2019.118263.
- [10] V.P. Indrakanti, J.D. Kubicki, H.H. Schobert, Photoinduced activation of CO₂ on Ti-based heterogeneous catalysts: current state, chemical physics-based insights and outlook, *Energy Environ. Sci.*, 2 (2009) 745–758.
- [11] H. Ma, B. Wang, X. Luo, Studies on degradation of methyl orange wastewater by combined electrochemical process, *J. Hazard. Mater.*, 149 (2007) 492–498.
- [12] I. Ihsanullah, A. Jamal, M. Ilyas, M. Zubair, G. Khan, M.A. Atieh, Bioremediation of dyes: current status and prospects, *J. Water Process Eng.*, 38 (2020) 101680, doi: 10.1016/j.jwpe.2020.101680.
- [13] J.O. Ighalo, O.J. Ajala, A.G. Adeniyi, E.O. Babatunde, M.A. Ajala, Ecotoxicology of glyphosate and recent advances in its mitigation by adsorption, *Environ. Sci. Pollut. Res.*, 28 (2021) 2655–2668.
- [14] D.A. Giannakoudakis, N. Farahmand, D. Omot, K. Sobczak, T.J. Badosz, J.C. Colmenares, Ultrasound-activated TiO₂/GO-based bifunctional photoreactive adsorbents for detoxification of chemical warfare agent surrogate vapors, *Chem. Eng. J.*, 395 (2020) 125099, doi: 10.1016/j.cej.2020.125099.
- [15] Z. Huang, P. Dong, Y. Zhang, X. Nie, X. Wang, X. Zhang, A ZIF-8 decorated TiO₂ grid-like film with high CO₂ adsorption for CO₂ photoreduction, *J. CO₂ Util.*, 24 (2018) 369–375.
- [16] S. Zhang, J. Wang, Y. Zhang, J. Ma, L. Huang, S. Yu, L. Chen, G. Song, M. Qiu, X. Wang, Applications of water-stable metal-organic frameworks in the removal of water pollutants: a review, *Environ. Pollut.*, 291 (2021) 118076, doi: 10.1016/j.envpol.2021.118076.
- [17] Y. Liu, D. Lin, W. Yang, X. An, A. Sun, X. Fan, Q. Pan, In situ modification of ZIF-67 with multi-sulfonated dyes for great enhanced methylene blue adsorption via synergistic

- effect, *Microporous Mesoporous Mater.*, 303 (2020) 110304, doi: 10.1016/j.micromeso.2020.110304.
- [18] L.L. Tan, W.J. Ong, S.P. Chai, B.T. Goh, A.R. Mohamed, Visible-light-active oxygen-rich TiO₂ decorated 2D graphene oxide with enhanced photocatalytic activity toward carbon dioxide reduction, *Appl. Catal., B*, 179 (2015) 160–170.
- [19] J. Zhang, Y. Cai, K. Liu, Extremely effective boron removal from water by stable metal organic framework ZIF-67, *Ind. Eng. Chem. Res.*, 58 (2019) 4199–4207.
- [20] W. Guan, X. Gao, G. Ji, Y. Xing, C. Du, Z. Liu, Fabrication of a magnetic nanocomposite photocatalysts Fe₃O₄@ZIF-67 for degradation of dyes in water under visible light irradiation, *J. Solid State Chem.*, 255 (2017) 150–156.
- [21] T. Li, M. Lu, Y. Gao, X. Huang, G. Liu, D. Xu, Double layer MOFs M-ZIF-8@ZIF-67: the adsorption capacity and removal mechanism of fipronil and its metabolites from environmental water and cucumber samples, *J. Adv. Res.*, 24 (2020) 159–166.
- [22] R. Li, W. Li, C. Jin, Q. He, Y. Wang, Fabrication of ZIF-8@TiO₂ micron composite via hydrothermal method with enhanced absorption and photocatalytic activities in tetracycline degradation, *J. Alloys Compd.*, 825 (2020) 154008, doi: 10.1016/j.jallcom.2020.154008.
- [23] M. Zhang, Q. Shang, Y. Wan, Q. Cheng, G. Liao, Z. Pan, Self-template synthesis of double-shell TiO₂@ZIF-8 hollow nanospheres via sonocrystallization with enhanced photocatalytic activities in hydrogen generation, *Appl. Catal., B*, 241 (2018) 149–158.
- [24] K.Y.A. Lin, H.A. Chang, Zeolitic imidazole framework-67 (ZIF-67) as a heterogeneous catalyst to activate peroxymonosulfate for degradation of Rhodamine B in water, *J. Taiwan Inst. Chem. Eng.*, 53 (2015) 40–45.
- [25] H.R. Pouretedal, N. Sadegh, Effective removal of Amoxicillin, Cephalixin, Tetracycline and Penicillin G from aqueous solutions using activated carbon nanoparticles prepared from vine wood, *J. Water Process Eng.*, 1 (2014) 64–73.
- [26] H.N. Tran, S.J. You, H.P. Chao, Thermodynamic parameters of cadmium adsorption onto orange peel calculated from various methods: a comparison study, *J. Environ. Chem. Eng.*, 4 (2016) 2671–2682.
- [27] A.W. Tan, A.L. Ahmad, B.H. Hameed, Adsorption of basic dye on high-surface-area activated carbon prepared from coconut husk: equilibrium, kinetic and thermodynamic studies, *J. Hazard. Mater.*, 154 (2008) 337–346.
- [28] H.N. Tran, S.J. You, A. Hosseini-Bandegharai, H. Chao, Mistakes and inconsistencies regarding adsorption of contaminants from aqueous solutions: a critical review, *Water Res.*, 120 (2017) 88–116.
- [29] K.V. Kumar, Comments on “Adsorption of acid dye onto organobentonite”, *J. Hazard. Mater.*, 137 (2006) 638–639.
- [30] Q. Yang, R. Lu, S. Ren, C. Chen, Z. Chen, X. Yang, Three dimensional reduced graphene oxide/ZIF-67 aerogel: Effective removal cationic and anionic dyes from water, *Chem. Eng. J.*, 348 (2018) 202–211.
- [31] W. Hassan, U. Farooq, M. Ahmad, M. Athar, M.A. Khan, Potential biosorbent, *Haloxylon recurvum* plant stems, for the removal of methylene blue dye, *Arabian J. Chem.*, 10 (2017) 1512–1522.
- [32] Z. Zhang, J. Zhang, J. Liu, Z. Xiong, X. Chen, Selective and competitive adsorption of azo dyes on the metal-organic framework ZIF-67, *Water Air Soil Pollut.*, 227 (2016) 471–482.
- [33] Y. Liu, D. Lin, W. Yang, X. An, A. Sun, X. Fan, Q. Pan, *In-situ* modification of ZIF-67 with multi-sulfonated dyes for great enhanced methylene blue adsorption via synergistic effect, *Microporous Mesoporous Mater.*, 303 (2020) 110304, doi: 10.1016/j.micromeso.2020.110304.
- [34] Z. Mahdi, Q.J. Yu, A.E. Hanandeh, Investigation of the kinetics and mechanisms of nickel and copper ions adsorption from aqueous solutions by date seed derived biochar, *J. Environ. Chem. Eng.*, 6 (2018) 1171–1181.

Supplementary information

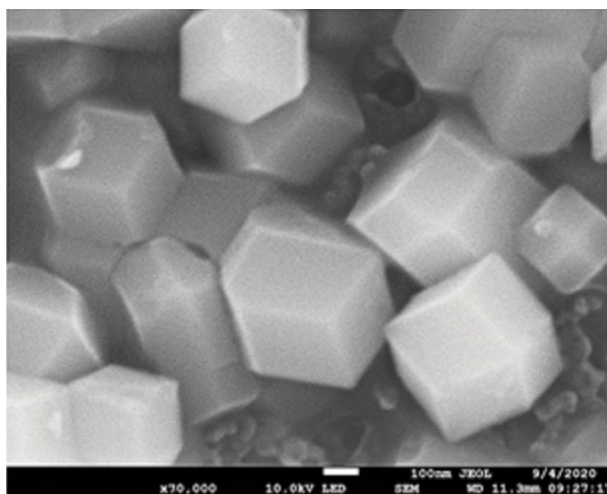


Fig. S1. SEM image of ZIF-67.

Table S1
MO maximum adsorption capacity Q_{\max} of various adsorbents calculated from Langmuir model and experiment condition

Adsorbent	Q_{\max} (mg g ⁻¹)	pH	Temperature (°C)	SSA (m ² g ⁻¹)	Reference
Polyethyleneimine-modified persimmon tannin	877.2	4.0	50	8.1	[S1]
AC from waste tire rubber	588.0	3.6	23	–	[S2]
Activated biochar from pomelo peel waste	163.1	3.0	25	75.3	[S3]
Calcined glycerol-modified nanocrystalline MgAl LDH	1062	4.50	25	170.3	[S4]
Cd-based MOF	166.7	7.0	25	384.0	[S5]
Immobilised polyaniline	77.50	6.5	30	8.5	[S6]
Mesoporous MCM-41	1,000	2.0	20	1,451	[S7]
Immobilised chitosan/montmorillonite G	154.4	6.3	30	4.4	[S8]
LDH/Fe ₃ O ₄ /polyvinyl alcohol G (A-F)	19.59	6.0	25	87	[S9]
ZIF-67	1,340	6.5	25	1,676	[S10]

SSA – specific surface area.

Part S1

The first-order kinetic model for adsorption can be expressed as [S11]:

$$\ln(Q_e - Q_t) = \ln Q_e - k_1 t \quad (S1)$$

where k_1 (g mg⁻¹ h⁻¹) is the adsorption rate constant.

Table S2
Parameters from fitting the experimental data of TiO₂@ZIF-67 with first-order model

C_0	$Q_{e,exp}$	First-order		
		$Q_{e,cal}$	k_1	R^2
mg L ⁻¹	mg g ⁻¹	mg g ⁻¹	g mg ⁻¹ h ⁻¹	
1	1.07	0.02	1.09	0.7994
2.5	2.83	0.47	1.43	0.9642
5	5.83	0.81	1.59	0.9579

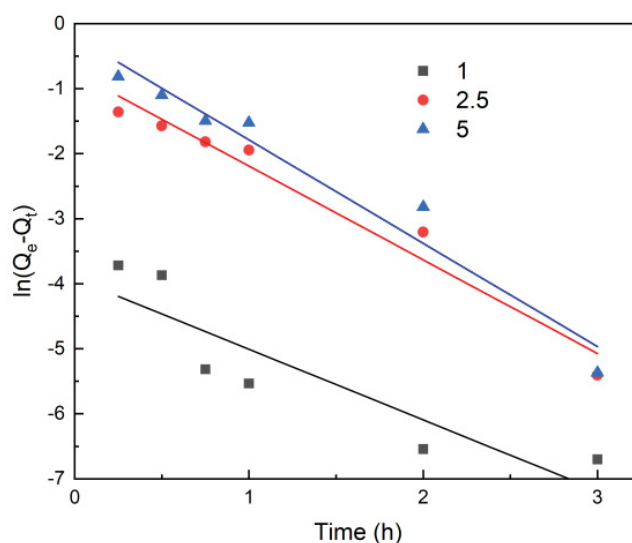
Fig. S2. Fitting of first-order model of MO adsorption on TiO₂@ZIF-67.

Table S3
Parameters from fitting the experimental data of TiO₂@ZIF-67 with second-order model

C ₀	Q _{e,exp}	Second-order		
		Q _{e,cal}	k ₂	R ²
mg L ⁻¹	mg g ⁻¹	mg g ⁻¹	g mg ⁻¹ h ⁻¹	
1	1.07	1.08	129.78	0.9998
2.5	2.83	2.84	3.22	0.9998
5	5.83	5.85	5.80	0.9999

Part S2

The expression of Langmuir model as follow [S12]:

$$\frac{C_e}{Q_e} = \frac{C_e}{Q_{max}} + \frac{1}{Q_{max}K_L} \tag{S2}$$

where K_L, the Langmuir isotherm constant, is related to the adsorption bonding energy, and Q_{max} is the estimated maximal adsorption capacity. The fitting results showed the Langmuir isotherm model could not describe the adsorption process well (Fig. S1 and Table S2), since the R² values obtained by fitting at different temperatures 0.236,

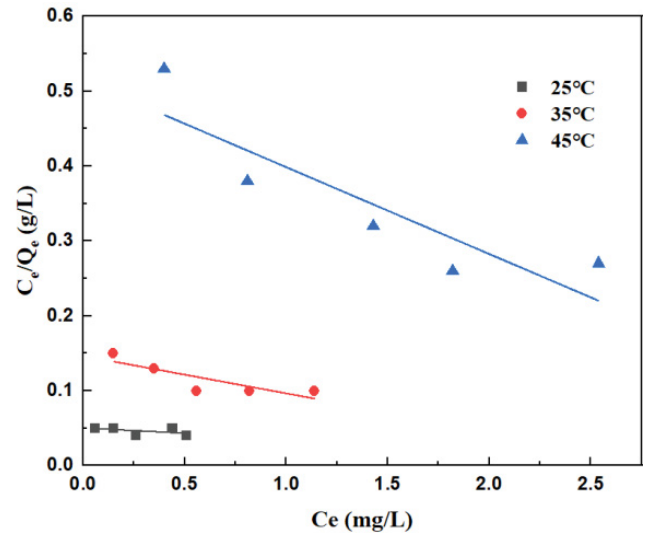


Fig. S3. Fitting of Langmuir isotherms of MO adsorption on TiO₂@ZIF-67.

0.715 and 0.780 at temperature of 25°C, 35°C and 45°C, respectively.

Part S3

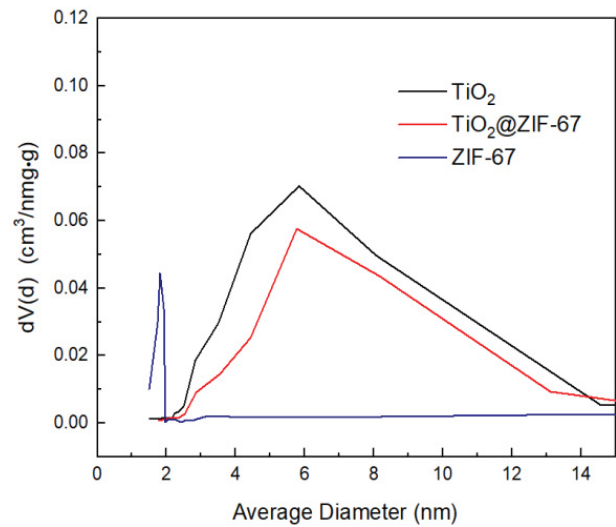
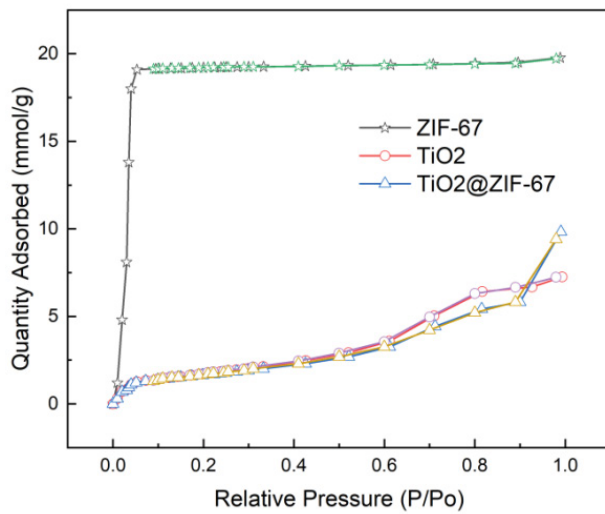


Fig. S4 (a) N₂ sorption–desorption isotherms and (b) pore-size distributions of three materials (Note: the color marked in Fig. 4a is for adsorption and the different color is for desorption).

References

- [S1] X. Li, Z. Wang, J. Ning, M. Gao, W. Jiang, Z. Zhou, G. Li, Preparation and characterization of a novel polyethyleneimine cation-modified persimmon tannin bioadsorbent for anionic dye adsorption, *J. Environ. Manage.*, 217 (2018) 305–314.
- [S2] M.T. Islam, R. Saenz-Arana, C. Hernandez, T. Guinto, M.A. Ahsan, D.T. Bragg, H. Wang, B. Alvarado-Tenorio, J.C. Noveron, Conversion of waste tire rubber into a high-capacity adsorbent for the removal of methylene blue, methyl orange, and tetracycline from water, *J. Environ. Chem. Eng.*, 6 (2018) 3070–3082.
- [S3] B. Zhang, Y. Wu, L. Cha, Removal of methyl orange dye using activated biochar derived from pomelo peel wastes: performance, isotherm, and kinetic studies, *J. Dispersion Sci. Technol.*, 41 (2019) 125–136.
- [S4] W. Yao, S. Yu, J. Wang, Y. Zou, S. Lu, Y. Ai, N.S. Alharbi, A. Alsaedi, T. Hayat, X. Wang, Enhanced removal of methyl orange on calcined glycerol-modified nanocrystalline Mg/Al layered double hydroxides, *Chem. Eng. J.*, 307 (2017) 476–486.
- [S5] A.C. Tella, M.D. Olawale, M. Neuburger, J.A. Obaleye, Synthesis and crystal structure of Cd-based metal-organic framework for removal of methyl-orange from aqueous solution, *J. Solid State Chem.*, 255 (2017) 157–166.
- [S6] N.N. Bahrudin, M.A. Nawawi, W.I.N.W. Ismail, Physical and adsorptive characterizations of immobilized polyaniline for the removal of methyl orange dye, *Korean J. Chem. Eng.*, 35 (2018) 1450–1461.
- [S7] T.M. Albayati, G.M. Alwan, O.S. Mahdy, High performance methyl orange capture on magnetic nanoporous MCM-41 prepared by incipient wetness impregnation method, *Korean J. Chem. Eng.*, 34 (2016) 259–265.
- [S8] N.N. Bahrudin, M.A. Nawawi, A.H. Jawad, S. Sabar, Adsorption characteristics and mechanistic study of immobilized chitosan-montmorillonite composite for methyl orange removal, *J. Polym. Environ.*, 28 (2020) 1901–1913.
- [S9] S. Mallakpour, M. Hatami, An effective, low-cost and recyclable bio-adsorbent having amino acid intercalated LDH@Fe₃O₄/PVA magnetic nanocomposites for removal of methyl orange from aqueous solution, *Appl. Clay Sci.*, 174 (2019) 127–137.
- [S10] Z. Zhang, J. Zhang, J. Liu, Z. Xiong, X. Chen, Selective and competitive adsorption of azo dyes on the metal-organic framework ZIF-67, *Water Air Soil Pollut.*, 227 (2016) 471–482.
- [S11] Z. Liu, X. Chen, L. Zhou, P. Wei, Development of a first-order kinetics-based model for the adsorption of nickel onto peat, *Min. Sci. Technol. (CN)*, 19 (2009) 230–234.
- [S12] H.N. Tran, C.C. Lin, S.H. Woo, H.C. Chao, Efficient removal of copper and lead by Mg/Al layered double hydroxides intercalated with organic acid anions: adsorption kinetics, isotherms, and thermodynamics, *Appl. Clay Sci.*, 154 (2018) 17–27.